Journal of the European Ceramic Society **18** (1998) 751–758

PII: S0955-22197-001842
0955-2219/98/$19.00 + 0.00

A Transmission Electron Microscope Study of Commercial X7R-Type Multilayer Ceramic Capacitors

F. Azough, R. Al-Saffar and R. Freer*

Materials Science Centre, University of Manchester/UMIST, Grosvenor Street, Manchester, UK, M1 7HS

(Received 28 August 1997; accepted 22 October 1997)

Abstract

X7R-type multilayer ceramic capacitors produced by three commercial manufacturers (A, B and C) have been investigated by transmission electron microscopy. All the specimens contained grains with distinct core–shell structures; the cores were almost pure $BaTiO_3$ and exhibited domain structures at room temperature. Specimens of type A had a grain size of 1–2 μm, with 'wide' shells containing Pb, Bi, Nb, Ba and Ti. A bonding phase, rich in Si, Al, Ba and Ti was detected between the dielectric grains and Ag–Pd electrodes. Heating the samples to temperatures above 130°C caused the ferroelectric domain structure to be lost and replaced by a dislocation network. Specimens of type B and C had a grain size of 0·5–1·0 μm; the ferroelectric cores were surrounded by 'narrow' shells rich in Nb, Co, Ba and Ti. The Ag–Pd internal electrodes were twinned. Type I and type II core–shell structures were found in all three sets of multilayer ceramic capacitors. © *1998 Elsevier Science Limited. All rights reserved*

1 Introduction

Ferroelectric barium titanate forms the basis of the majority of multilayer ceramic (MLC) capacitors, but with structural transitions, in the normal operational range at ~0°C and ~130°C, and a very large dielectric peak at ~130°C, additives are necessary to produce commercially-useful powder formulations.[1–3] For the X7R-type dielectrics the relative permittivity (ε_r) must not change by more than ±15% from the value at 25°C over the temperature range −55 to 125°C.[3,4] An important characteristic of X7R-type materials is the presence of core–shell structures within individual grains; the core is usually relatively pure tetragonal ferroelectric $BaTiO_3$ whilst the non-ferroelectric shells contain most of the additives.[1–3,5–9] The controlled structural inhomogeneity is usually achieved by pre-reacting the $BaCO_3$ and TiO_2 and then mixing with dopants prior to sintering; failure of the additives to fully interdiffuse leaves them trapped in the outer regions of the grains.[1–3] Dielectric stability, and the comparatively flat ε_r-temperature characteristic is due to the combination of the responses of the core and shell regions, or more strictly the many separate ε_r-temperature curves in the compositional gradient, each with its own Curie temperature.[1,3,8]

There are four main groups of additives for $BaTiO_3$:

1. isovalent, e.g. Sr for Ba, or Zr for Ti which tend to modify Curie temperature;[10]
2. donor dopants, with a charge greater than that of the host ion, e.g. Nb^{5+} for Ti^{4+}, and Nd^{3+} for Ba^{2+}; when present at $\geq 0{\cdot}5$ mol% they tend to inhibit grain growth;[11]
3. acceptor ions, e.g. Mg^{2+}, Ni^{2+} and Co^{2+} which replace Ti^{4+}; they tend to partly counteract the effect of donor dopants but also improve donor solubility in $BaTiO_3$. An additional benefit is that they assist dielectric-temperature stability;[12]
4. low-melting glass compositions[13,14]—the most common ones are summarised in Table 1, but include Bi_2O_3, PbO, SiO_2, Al_2O_3 and B_2O_3.

Core-shell structures have been observed in a number of $BaTiO_3$-based, model systems, including those with addition of ZrO_2,[6,7,15,16] $ZnO + Bi_2O_3$,[17] $CdBi_2Nb_2O_9$,[2] $Bi_4Ti_3O_{12}$,[1] $Bi_2O_3 + Nb_2O_5$[8,18] and

*To whom correspondence should be addressed. Fax: 0044-0161-200-3586; e-mail: Robert.Freer@umist.ac.uk

Table 1. The main oxides present in low melting temperature glass compositions (after Kahn *et al.*[3])

Major component	*Modifier component*	*Glass former*
PbO	ZnO	B_2O_3
Bi_2O_3	CdO	SiO_2
BaO	Al_2O_3	GeO_2

CeO_2.[9] Hennings and Rosenstein[2] suggested that the core and shell are not different phases but in fact coherent across the boundary. Subsequently, Armstrong and Buchanan[16] found that in ZrO_2-doped $BaTiO_3$ the expansion mismatch between core and shell generated internal stress which puts the core in compression. Lu *et al.*[6] identified three types of core–shell structures in zirconia-doped $BaTiO_3$: type I structures have ferroelectric domains and a featureless shell; type II structures have dislocations extending to the shell region co-existing with ferroelectric domains; type III structures have no ferroelectric domains but a high density of dislocations. They argued that if sintering was allowed to proceed for extended times then Zr would diffuse into the core and the compositional homogenisation would cause a transition from a type I structure to a type III structure. Cerium is also isovalent with Ti, and one of the less common dopants for X7R dielectrics.[19] CeO_2 additions to $BaTiO_3$ dramatically reduce the Curie temperature and give rise to a grain microstructure having three distinct regions: a small core of almost-pure $BaTiO_3$, a shell rich in Ce and an intermediate region with a concentration gradient of Ce/(Ba + Ti).

In X7R materials prepared with Nb_2O_5 and Bi_2O_3 there is much evidence to suggest that a liquid phase forms during sintering.[2,8,18] The subsequent reactions are less well understood, but it has been postulated that there is a reaction between $BaTiO_3$ and the additives, partial vapourisation of Bi_2O_3 and also diffusion of Bi into the pre-existing $BaTiO_3$ grains.[8]

With the background knowledge of core shell structures in various model $BaTiO_3$-based systems the present study is an investigation of the microstructure of three typical commerical X7R multilayer ceramic capacitors.

2 Experimental

Samples of X7R-type multilayer ceramic (MLC) capacitors were supplied by three commercial manufacturers. Hereafter, these will be designated as specimens A, B, C. The MLC capacitors were prepared by standard tape-casting techniques; individual components were typically 6×4×1 mm in size.

For TEM studies, specimens were prepared using a modified version of the technique employed by Reaney and Barber[20] for thin films. After removing termination electrodes by grinding, pairs of MLC capacitors were glued together with epoxy resin. Cores, 3 mm diameter were drilled from the composite assemblages. These were cut, then ground to a thickness of ~100 μm, and finally ion-milled (Ion Tech 791) to the required form. A Philips EM430 transmission electron microscope, operating at 300 keV, was used for microstructural studies. The TEM was equipped with an energy dispersive X-ray analytical system (EDS) for chemical analysis and a hot stage; the latter allowed samples to be heated to 150°C.

3 Results and Discussion

3.1 Sample A

Figure 1(a) is a typical TEM micrograph of sample A. It is predominantly single phase, with a grain size of 1–2 μm. The duplex core–shell structure,

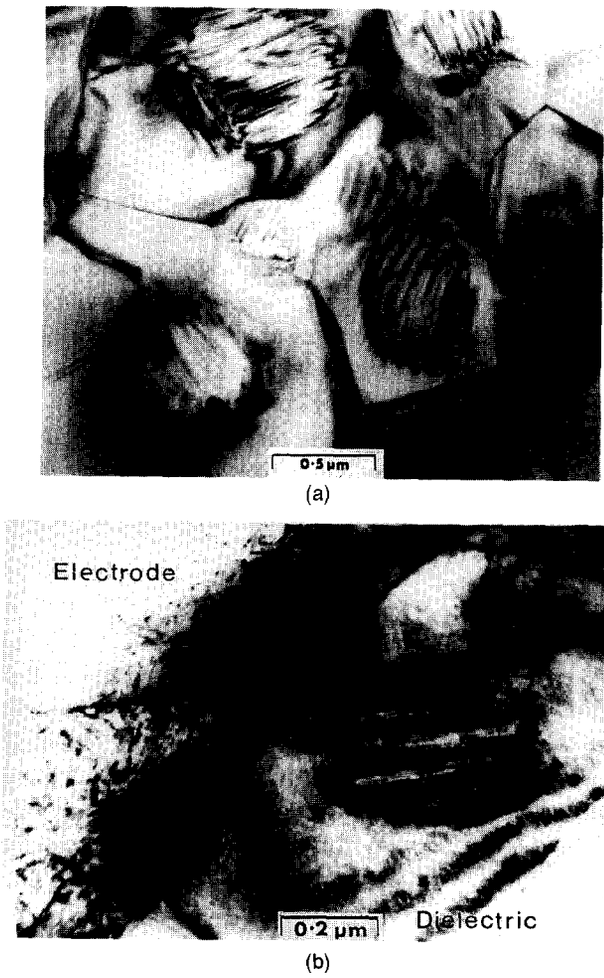

Fig. 1. (a) Low magnification TEM micrograph of sample of type A showing the grain size and duplex structure; (b) higher magnification TEM micrograph of sample of type A showing detail of the core–shell structure.

characteristic of X7R-type materials, is evident throughout the sample. Only type I and type II core–shell structures were observed. Figure 1(b) is a higher magnification TEM micrograph, showing detail of an individual core–shell structure; the internal electrode is visible at the left hand side of the figure.

Chemical analysis of the grains (EDS) showed that the cores were almost pure $BaTiO_3$, with traces of Nb and Pb, whilst the shells contained significant amounts of Nb, Pb and Bi.

A scanning transmission electron microscope (STEM) X-ray map for two adjacent grains is shown in Fig. 2 The TEM image of the grains is shown in the top left hand corner of the figure, and their individual elemental X-ray maps in the lower half of the figure. The bottom row shows the original (unprocessed) X-ray data, with the processed data immediately above. Comparison of the TEM image and the composite overlay of X-ray maps reveals that Nb, Bi and Pb are mainly located in the grain shells.

Whilst sample A was predominantly single phase $BaTiO_3$-based perovskite, occasional second phase grains were present. Figure 3 shows a lath-shaped grain, approximately 2·5 μm long and 0·5–1·0 μm wide. This grain is rich in Ti with small amounts of Nb (Fig. 3), and is believed to be a low melting temperature phase.

The internal electrodes were, as expected for an X7R MLC capacitor, based on a Ag–Pd alloy. Due to overlapping peaks in the EDS spectra, it is not possible to quantify the alloy composition. TEM imaging of the electrodes showed that they were frequently twinned (Fig. 4). At the interface between the twinned region and the dielectric, laminations or cracks were occasionally observed. This was not totally unexpected as internal bonding is not always perfect. However, in some areas, a thin layer, rich in (Si, Al, Ba and Ti) was found

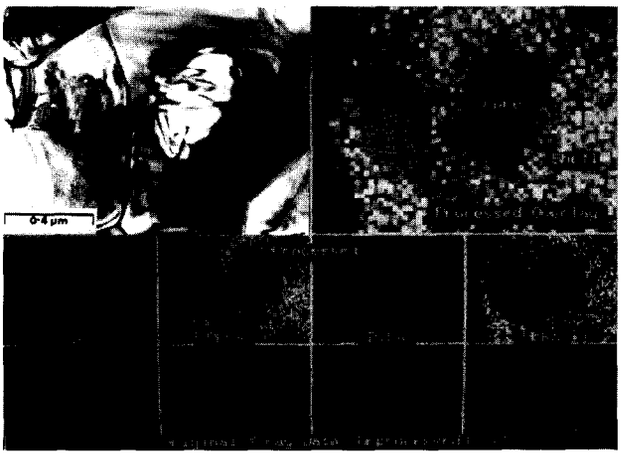

Fig. 2. TEM micrograph and X-ray maps for sample of type A (see text for details).

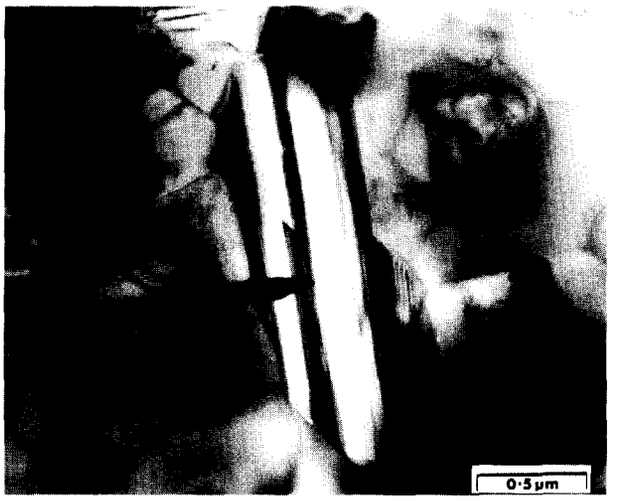

Fig. 3. TEM micrograph of second phase (arrowed) in sample of type A.

between the dielectric and the electrode (Fig. 5). This phase was up to 5 μm in length. The presence of comparatively large amounts of Si in the bond phase suggests that it formed from a low melting temperature glass during fabrication. TEM analysis revealed the existence of thickness fringes indicating the development of a crystalline form.

On heating, sample A showed good thermal stability. After heating to 150°C for 30 min and cooling to room temperature no lamination or cracking of the dielectric or dielectric–electrode interface was observed. Figure 6 shows a series of micrographs for sample A during thermal cycling. At room temperature [Fig. 6(a)], core–shell structures of type I are visible in both large (5 μm) and small ($\leq$ 1 μm) grains. At 120°C during heating [Fig. 6(b)] domain structures within the cores are still visible, but not so distinct as at room temperature. By 150°C all evidence of domains and core–shell structures was lost, and only dislocations could be

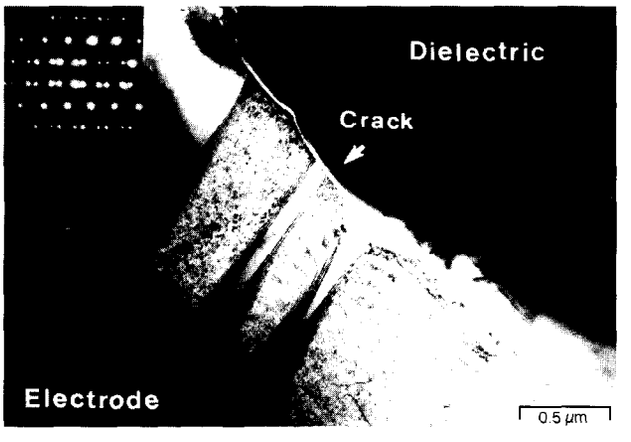

Fig. 4. TEM micrograph of sample of type A showing the internal electrode which is twinned, and lamination at the interface of the dielectric and the electrode. Inset is the electron diffraction pattern from the electrode confirming twinning in the electrode.

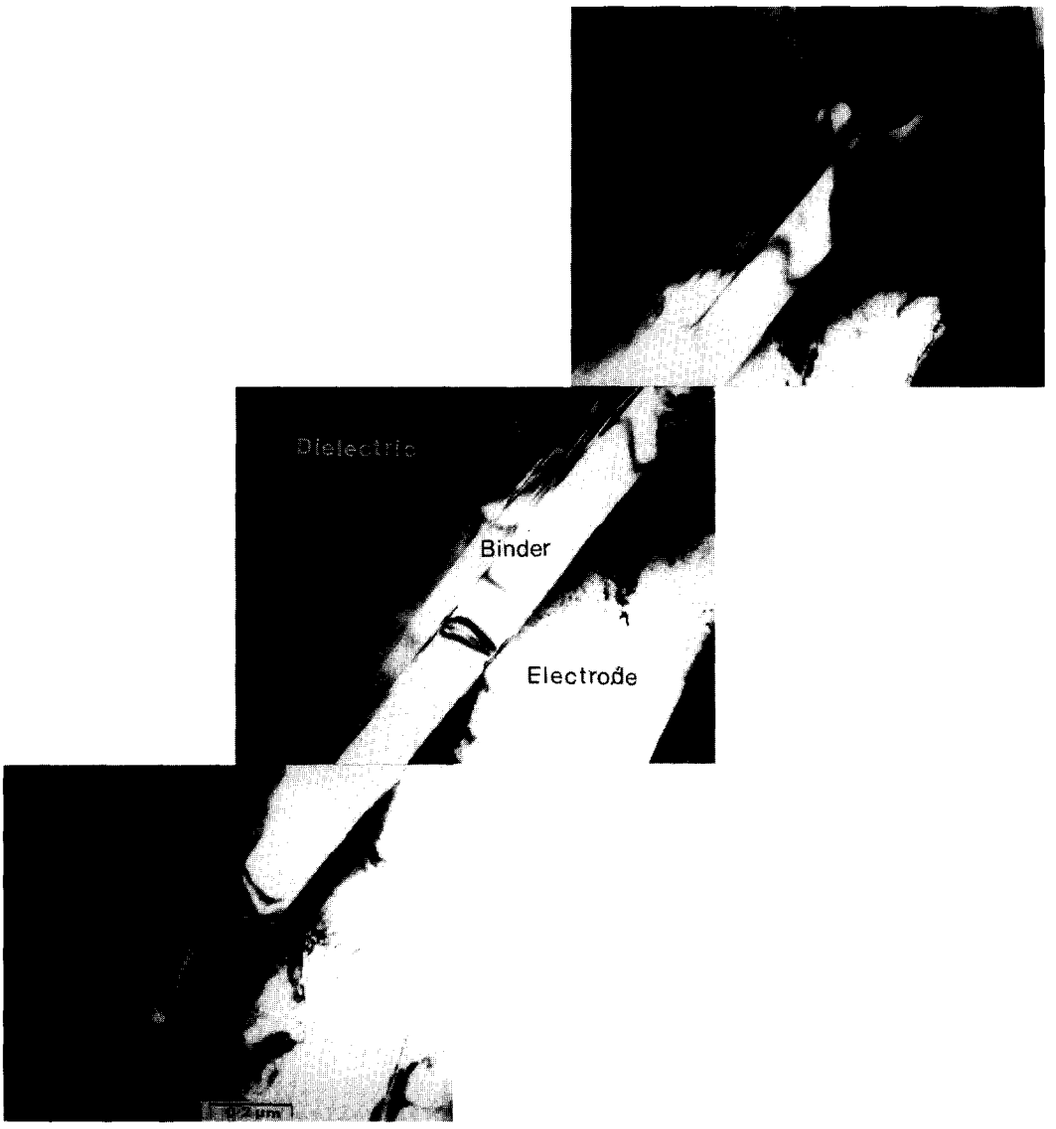

Fig. 5. TEM micrograph of sample of type A, showing a 'binder' phase between the dielectric and internal electrode.

seen [Fig. 6(c)]. During cooling the sequence of microstructural changes were reversed such that details of the domains were evident by 120°C [(Fig. 6(d)], and the core–shell structures were fully formed once more in the room temperature images [(Fig. 6(e)]. These images are very similar to those reported by Park and Song[9] for $BaTiO_3$–$0{\cdot}03CeO_2$:$1{\cdot}5TiO_2$ ceramics, and by Saucy *et al.* for $BaTiO_3$–ZrO_2 ceramics. For the CeO_2-doped samples, Park and Song found that the additives depressed the Curie temperature to ~50°C, with the result that the core–shell structures did not exist at 125°C and, during cooling, became increasingly stronger between 80°C and 25°C. Additions of ZrO_2 had only a minor effect on the upper (~130°C) transition temperature, but increased the lower (~0°C) transition temperature with the result that both merged at ~105°C in $BaTiO_3$ containing 5 wt% ZrO_2. Domain structures were clearly visible in the cores of $BaTiO_3$–2 wt% ZrO_2 grains up to 120°C.

3.2 Sample B

Sample B was again predominantly single phase perovskite, but with a smaller grain size of 0·5–1·0 μm [Fig. 7(a)]. At room temperature core shell structures are ubiquitous, with both type I and type II forms being present. Figure 7(b) shows detail of the domain structure in the core of a single grain. In general, the shells of grains in sample B were narrower than those in Sample A.

Chemical analysis of sample B showed that grain cores were almost pure $BaTiO_3$, whilst the shells contained small amounts of Nb and Co (Fig. 8). A second phase, rich in Co and Ti was found as individual large grains, typically $2{\times}0{\cdot}5\,\mu$m in size (Fig. 9). This is believed to be cobalt titanate, which is analogous to the zinc titanate grains occasionally found in zirconium tin titanates prepared with ZnO as a sintering aid.[21,22] Small $BaTiO_3$ particles were located within the second phase. Again, the second phase may have resulted from a liquid phase during fabrication.

Fig. 6. TEM micrographs showing core–shell structures in sample of type A during heating and cooling, at (a) room temperature, (b) 120°C, (c) 150°C, (d) 120°C, (e) room temperature.

3.3 Sample C

The third sample was very similar to sample B in that it had a small grain size, in the range 0·5 to 1·0 μm, and extensive duplex core–shell structures; both type I and type II structures were present in sample C, and the shells were narrow (Fig. 10). Niobium and cobalt were found in the grain shells in approximately the same amounts in sample B.

The second phase present in specimen C, in the form of large needle shaped grains (up to 10 μm by 14 μm), was rich in Ba, Ti, Si, Al and Co (Fig. 11). Small $BaTiO_3$ particles were found within the second phase.

3.4 Overview

Although samples B and C were produced by two different manufacturers it is clear that there are many similarities (Table 2). It is therefore convenient to group samples B and C together and compare directly with sample A. Both types of sample have been prepared with Nb additions. This donor dopant serves as a grain growth inhibitor, controlling grain size to approximately 1·0 μm, marginally smaller for samples B and C. Significant amounts of Nb were found in the shells of all grains. Samples B and C also contained the acceptor dopant cobalt. This should have

improved the solubility of Nb in $BaTiO_3$, as well as partly counteracting the effect of the donor dopant. To ensure that the dielectric can be sintered at a 'low' temperature (~1150°C) further additives are required to produce a liquid phase. For X7R materials silicate glasses are common. Comparison of Tables 1 and 2 suggests that the components of the liquid phase in sample A were oxides of Pb, Bi, Nb, Al and Si. In contrast samples B and C appear to have relied upon oxides of Nb, Si and Al to react with $BaTiO_3$ to develop the liquid phase.

Although it was apparent that the grain size of sample A was slightly larger than that of samples B and C, another notable feature was the wider shells

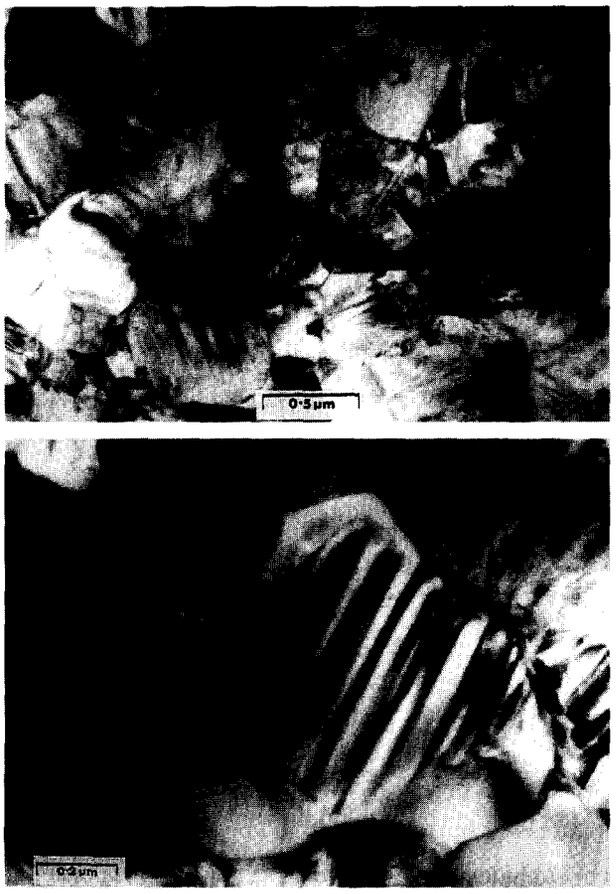

Fig. 7. TEM micrographs of sample of Type B showing (a) the grain size and duplex structure, and (b) detail of the core–shell structure (type I).

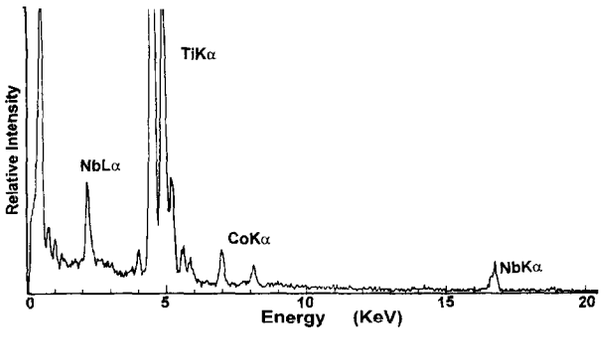

Fig. 8. EDS spectrum of shell of the grain shown in Fig. 7(b).

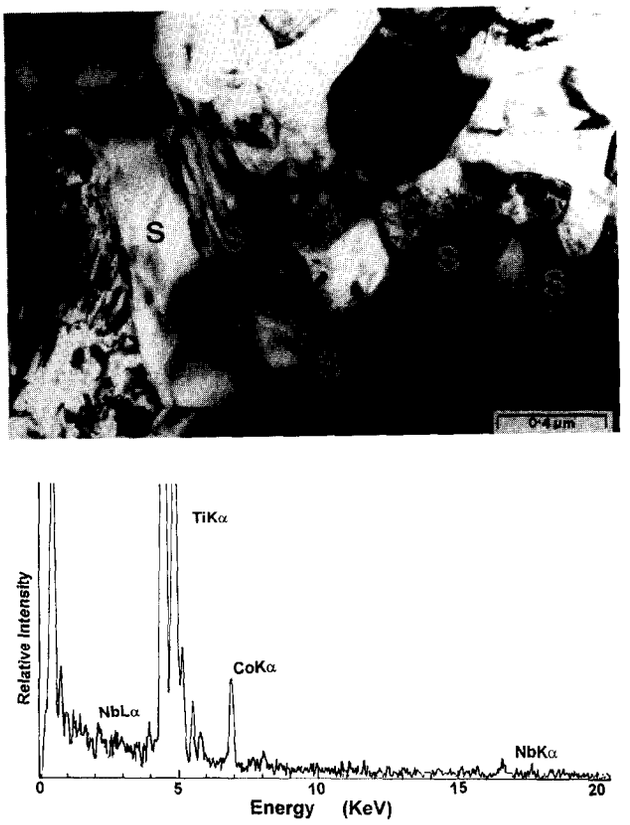

Fig. 9. (a) TEM micrograph of second phase (S) in sample of type B; (b) EDS spectrum of the second phase shown in (a).

Fig. 10. TEM micrographs of sample of type C showing (a) the overall microstructure; and (b) detail of core–shell structure.

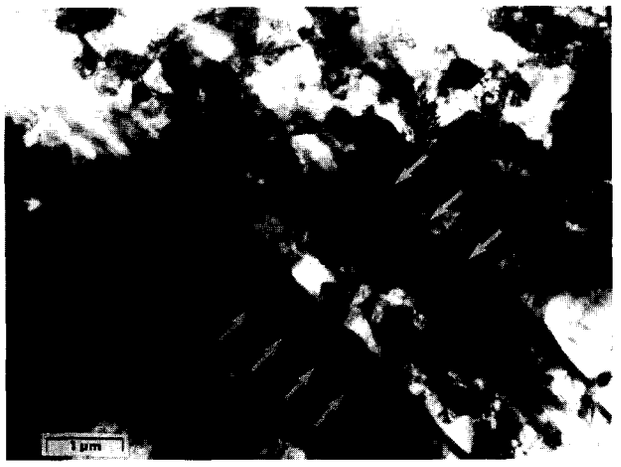

Fig. 11. TEM micrograph of second phase (arrowed) in sample of type C.

in sample A. Type I core–shell structures were ubiquitous in all samples, and type II structures were found occasionally. Type III structures (no ferroelectric domains but a high density of dislocations) were only observed when samples were heated above the Curie temperature, e.g. Fig. 6(c).

Second phases in the dielectrics were rare, but when present were generally in the shape of lamellae, several microns in length, e.g. Fig. 3. In sample A the second phases were mainly rich in Ba and Ti, with minor amounts of Pb, Nb and Bi. Between the dielectric and internal electrode there was another lamellar second phase, up to 5 μm in length, rich in Si, Al, Ba and Ti. This silicate phase, possibly a remnant from the liquid phase, may have served as a 'binder' between metal and ceramic. In samples B and C the second phases were of similar shape and contained a combination of Co, Si, Ti, Ba and Al. Again it is inferred that these grains developed from a liquid and are crystalline in nature.

Of the divalent substituting ions, Pb^{2+} tends to increase the 'upper' (~130°C) Curie temperatures in $BaTiO_3$, whilst Sr^{2+} tends to decrease both the upper and lower (~0°C) transition temperatures and Ca^{2+} decreases the lower transition temperature. The quadrivalent ions Zr and Sn tend to decrease the upper transition temperature but increase the lowest transition temperature, with the effect that they merge into single transitions at approximately 7% replacement by Zr and approximately 5% replacement by Sn.[10]

Within the small regions investigated the internal electrodes (Pd–Ag) were continuous and had apparent thicknesses of typically 0·4 μm (Fig. 5). In reality, the electrodes are 1–2 μm thick and tend to be 'net-shaped' with pillars of dielectric growing through the cavities, which improves the mechanical integrity of the devices.[23] Electron diffraction patterns revealed that the electrodes were twinned.

Table 2. Characteristics of commercial multilayer ceramic capacitors

Sample	*Grain size (μm)*	*Core–shell structures*	*Size of shell*	*Elements* in shell*	*Elements in second phase*
A	1–2	I and II	Wide	Pb,Bi,Nb	Nb,Pb,Bi,Ba,Ti, Si,Al,Ba,Ti +
B	0·5–1·0	I and II	Narrow	Nb,Co	Co, Ti
C	0·5–1·0	I and II	Narrow	Nb,Co	Si,Al,Co,Ba,Ti

*In addition to Ba and Ti.
+ Metal–ceramic 'bond' phase?

4 Conclusions

TEM investigations of commercial multilayer ceramic capacitors from three manufacturers revealed differences in terms of microstructure and the additives employed to achieve X7R-type characteristics:

1. Group A dielectrics had a grain size of 1–2 μm; the cores were almost pure $BaTiO_3$, whilst the wide shells contained Pb, Bi and Nb in addition to $BaTiO_3$. Secondary phases were rare but contained primarily oxides of Ba, Ti, Pb, Nb and Bi; between the dielectric and electrodes an Si–Al–Ba–Ti oxide phase was found. Both type I and type II core–shell structures were present. Nb is a donor dopant in $BaTiO_3$; the sintering process was aided by a liquid phase involving Nb, Pb, Bi, Al, Si, Ba and Ti oxides. Heating the samples to temperatures above 130°C caused the ferroelectric domain structure to be lost and replaced by a network of dislocations.
2. Group B and C dielectrics had grain sizes of 0·5–1·0 μm; the ferroelectric $BaTiO_3$ cores were surrounded by narrow shells containing Nb, Co, Ba and Ti oxides. Lamellar second phases contained Ba, Ti, Si, Al and Co. In these ceramics, Nb was a donor and Co an acceptor. Liquid phase sintering was aided by reactions involving some or all of Ba, Ti, Si, Al, Co and Nb oxides.
3. The internal electrodes were Ag–Pd; electron diffraction patterns confirmed that the metallic alloy was twinned.

References

1. Rawal, B. S., Kahn, M. and Bussem, W. R., Grain core–grain shell structure in barium titanate-based ceramics. In *Advances in Ceramics*, Vol. 1, ed. L. M. Levinson. American Ceramic Society, OH, Westerville, 1981, pp. 172–188.
2. Hennings, D. and Rosenstein, G. J., Temperature-stable dielectrics based on chemically inhomogeneous $BaTiO_3$. *J. Am. Ceram. Soc.*, 1984, **67**, 249–254.
3. Kahn, M., Burks, D. P., Burn, I. and Schulze, W. A., Ceramic capacitor technology. In *Electronic Ceramics—*

Properties, Devices and Applications, ed. L. M. Levinson, Marcel Dekker, New York, 1988, pp. 191–274.
4. Electronic Industries Association, specification #RS198.
5. Daniels, J. and Hardtl, K., Electrical conductivity at high temperature for donor-doped barium titanate ceramics. *Philips Res. Reports*, 1976, **31**, 489–504.
6. Lu, H., Bow, J. S. and Deng, W-H., J. Core–shell structures in ZrO_2 modified $BaTiO_3$ ceramic. *J. Am. Ceram. Soc.*, 1990, **73**, 3562–3568.
7. Saucey, C., Reaney, I. M. and Bell, A. J., Microstructure and electromechanical properties of $BaTiO_3$–ZrO_2 core–shell ceramics. *Br. Ceram. Proc.*, 1993, **51**, 31–52.
8. Pathumarak, S., Al-Khafaji, M. and Lee, W. E., Microstructure development on firing Nb_2O_5 and Bi_2O_3 doped $BaTiO_3$. *Br. Ceram. Trans.*, 1994, **93**, 114–118.
9. Park, Y. and Song, S. E., Influence of core–shell structured grain on dielectric properties of cerium-modified barium titanate. *J. Mater. Sci. Electronics*, 1995, **6**, 380–388.
10. Gaffe, B., Cook, W. R. and Gaffe, H., *Piezoelectric Ceramics*. Academic Press, London, 1971, p. 53.
11. Kahn, M., Influence of grain growth on dielectric properties of Nb-doped barium titanate. *J. Am. Ceram. Soc.*, 1971, **54**, 455–457; Preparation of small-grained and large-grained ceramics from Nb-doped $BaTiO_3$. *J. Am. Ceram. Soc.*, 1971, **54**, 452–454.
12. Burn, I., Temperature stable barium titanate ceramics containing niobium pentoxide. *Electrocomp. Sci: Technol.*, 1976, **2**, 241.
13. Maher, G. H., Improved dielectrics for multilayer ceramic capacitors. Proceedings of 27th Electronic Components Conference, IEEE, Arlington, VA, 1977, pp. 391–399.
14. Burn, I., Flux-sintered barium titanate dielectrics. *J. Mater. Sci*, 1982, **17**, 1398–1408.
15. Hennings, D., Schnell, A. and Simon, G., Diffuse ferroelectric phase transition in $Ba(Ti_{1-y}Zr_y)O_3$ ceramics. *J. Am. Ceram. Soc.*, 1982, **65**, 539–544.
16. Armstrong, T. R. and Buchanan, R. C., Influence of core–shell grains on the internal stress state and permittivity response of zirconia modified barium titillate. *J. Am. Ceram. Soc.*, 1990, **73**, 1268–1273.
17. McCartney, M. L., Sinclair, R. and Ewell, G. J., Chemical and microstructural analysis of grain boundaries in $BaTiO_3$-based dielectrics. In *Advances in Ceramics*, Vol. 1, ed. L. M. Levinson. American Ceramic Society, Westerville, OH, 1981, pp. 207–214.
18. Chiang, S. K., Lee, W. E. and Readey, D. W., Core-shell structure in doped $BaTiO_3$. *Am. Ceram. Soc. Bull.*, 1987, **66**, 1230.
19. Choi, C. J. and Park, Y., The X7R phenomenon in the core–shell structured ceramics. In *Ceramic Transactions* Vol. 8, ed. K. M. Nair, J. P. Guha and A. Okamoto. American Ceramic Society, Westerville, OH, 1990, pp.148–156.
20. Reaney, I. M. and Barber, D. J., Microstructural characterization of ferroelectric thin films in transverse section. *J. Am. Ceram. Soc.*, 1991, **74**, 1635–1638.
21. Wakino, K., Minai, K. and Tamura, H., Microwave characteristics of $(Zr,Sn)TiO_4$ and BaO–PbO–Nd_2O_3–TiO_2 dielectric resonators. *J. Am. Ceram. Soc.*, 1984, **67**, 278–281.
22. Azough, F., Microstructural development and microwave dielectric properties of ceramics in the system zirconia–titania–tin oxide. Ph.D Thesis, University of Manchester, 1991.
23. Al-Saffar, R., Freer, R., Tribick, I. and Ward, P., The mechanical properties of multilayer ceramic capacitors. In Proceedings CARTS-EUROPE '90, 1990, 191–198.